Curvature control in radial-axial ring rolling ⋆

Matthew R. Arthington * **Christopher J. Cleaver** ** **Jianglin Huang** * **Stephen R. Duncan** *

* *Dept of Engineering Science, 17 Parks Road, Oxford, OX1 3PJ, UK (e-mail: matthew.arthington@eng.ox.ac.uk).*
** *Dept of Engineering, Cambridge, CB2 1PZ, UK*

Abstract: Radial-axial ring rolling (RARR) is an industrial forging process that produces seamless metal rings with uniform cross-section using one radial and one axial rolling stage. Conventionally, the ring products are circular and the process is tightly constrained using guide rolls for stability, and to ensure the circularity and uniformity of the ring. Recent work has shown that when guide rolls are omitted, stability can be maintained using differential speed control of the roll pairs. However, achieving uniform curvature in this unconstrained configuration was not always possible when the controller only centred the ring within the rolling mill. In addition to the regulation of constant curvature in circular rings, differential speed control in unconstrained rolling offers an opportunity to bend the ring about the mandrel to create shapes with non-uniform curvature, for example: squares, hexagons, rings with flat sections, etc. We describe a control technique for creating non-circular rings using the rolling hardware of a conventional RARR mill, machine-vision sensing and differential speed control of the rolling stages. The technique has been validated for an industrial material in numerical simulations using the finite element method and also demonstrated on a desktop-scale RARR mill using modelling clay to simulate metal at elevated process temperatures.

Keywords: Process automation, process control, sensor systems, image processing, industrial control, forging, rolling

1. INTRODUCTION

Conventional radial-axial ring rolling (RARR) of cylindrical rings is an industrial forging process that produces seamless circular rings of metal with uniform cross-section, ASM (1988). A cylindrical ring of metal is rolled repeatedly by two rolling stages so that its wall thickness reduces and its diameter increases. Figure 1 provides a schematic overview of the process; a pair of cylindrical rollers (the mandrel and the forming roll) apply compressive forces to the radial faces; another pair of conical rollers (axial rolls) apply a compressive force to the faces of the ring. The forming roll and the conical rollers are driven to rotate the ring by friction, the mandrel is driven linearly but rotates freely. Conventional RARR mills also use two additional guide rolls to apply a radial force to help keep the centre of the ring aligned with the machine and achieve constant curvature in the XY plane (hereafter referred to as curvature), as shown in Figure 1. In this paper we restrict the processing parameters to a constant axial-roll separation.

Much research on ring rolling has focused on achieving the desired outcomes in the conventional process, Allwood et al. (2005) and Allwood et al. (2004). More recently, work has been published on developing machine-vision sensing to provide feedback on the current geometrical state, Meier et al. (2010), Arthington et al. (2014). This has led to improvements in monitoring the deformation state of the ring *in-situ* and also to the novel use of RARR to produce rings with variable radial wall thickness, Arthington et al. (2015). Amongst others, Arthington et al. (2015) showed

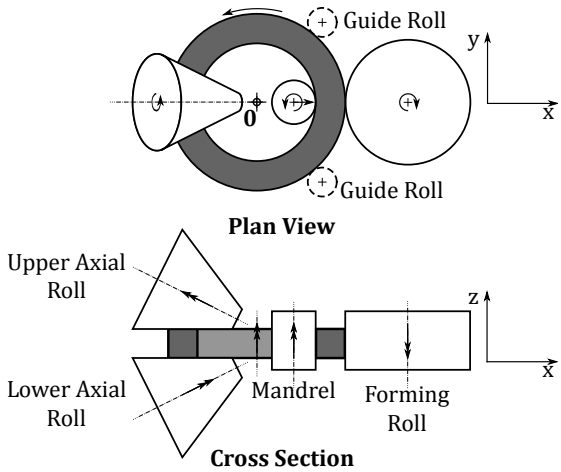

Fig. 1. A schematic diagram of the conventional RARR forging process showing the rolled ring shaded in grey. The radial roll gap is the region of the ring between the mandrel and the forming roll. The centre of the machine is taken as the origin, **0**, and is initially coincident with the axis of the ring.

⋆ This work was funded by the Engineering and Physical Sciences Research Council (EPSRC) UK.

that the stabilising and centring function of the guide rolls could be replicated by controlling the relative driving speeds of the forming and axial rolls to keep the ring centred with respect to the machine, potentially removing the need for guide rolls.

Moon et al. (2008) presented a study into (radial-only) ring rolling *with* guide rolls that investigated the formation of polygonal shapes in rolled rings when the forming ratio (mandrel feed rate vs forming roll speed) exceeded a critical value. In Moon et al. (2008)'s study, these polygonal shapes were considered defects to be avoided, however non-circular rings represent a class of rolled ring products that have various applications, and the advantages of ring rolling - fast production speeds, material savings, uniform material properties, etc. - could be used to make savings in time, energy, material and labour over other production techniques.

In ideal conventional rolling the value of the moment required for circular ring curvature changes smoothly throughout the process. However, disturbances from sources such as variable thickness, changing contact conditions, irregular heating, material variations, and dynamic instabilities can apply unforeseen loads to the ring, resulting in non-circular curvature that may not be corrected by simply centring the ring.

In this paper, we demonstrate control of the ring curvature to create specifically shaped rings with uniform wall thickness. This technique makes ring rolling a significantly more flexible process and also offers a way to regulate circular curvature more quickly than a centring-only approach.

The curvature of the segment of ring inside the radial roll gap region is altered by instructing the axial roll pair to change its feed speed relative to the feed speed of the forming roll. This action applies a bending moment about the mandrel. Along with the compressive radial force in the radial roll gap, the applied bending moment creates a plastic hinge, where the ring exhibits a permanent change in curvature. The size of the change in curvature depends on the angle of rotation of the plastic hinge, and is controlled by prescribing the Y_c coordinate of the centre of the ring, which must be positioned by the differential speeds of the rolling stages.

The deliberate actuation of the ring curvature (using this method or otherwise) has not previously been seen in the literature. With the potential to create shaped rings using conventional RARR rolling hardware the process can be used to produce a great variety of rolled-ring products.

2. SENSING

The sensing of the ring geometry permits the controller to actuate the rolls relative to the material in the ring. In conventional ring rolling, sensors are usually limited to measuring the bulk state of the ring, such as its diameter and thickness. In this section we provide a brief overview of the sensing technique and the procedure for creating variable thickness rings; more details can be found in Arthington et al. (2014) and Arthington et al. (2015).

2.1 Measuring current state of ring geometry

The sensor used in this process is a calibrated optical camera, which is trained on the XY plane of the ring. From this vantage, the upper surface of the ring is visible against a contrasting dark background. What follows is a description of the processing that takes place for each frame acquired by the camera.

First, the inner and outer edges of the ring wall are located using standard edge detection techniques, as described in Arthington et al. (2014). Once found, geometric shape parameters for the ring can be computed. Initially, ellipses are fitted to the inner and outer edges (which are not necessarily circular), which allows an approximate measure of the ring centre, $\mathbf{c}_0$, to be obtained from the mean of their centres. The radii of the inner and outer edges, $\mathbf{r}_{i0}(\theta) = [x_{i0}(\theta), y_{i0}(\theta)]^T$ and $\mathbf{r}_{o0}(\theta) = [x_{o0}(\theta), y_{o0}(\theta)]^T$, measured from $\mathbf{c}_0$ are calculated as functions of angle from the X axis. An approximate 'midline' [1] is computed using the mean radius, $\mathbf{m}_0(\theta) = (\mathbf{r}_{i0}(\theta)+\mathbf{r}_{o0}(\theta))/2$. An improved estimate of the ring centre is then found,

$$\mathbf{c}_1 = [X_c, Y_c]^T = \overline{\mathbf{m}}_0(\theta), \tag{1}$$

the radii recalculated and a more accurate midline, $\mathbf{m}_1(\theta)$, computed using the same method.

Calculating $\mathbf{m}_1(\theta)$ in this way can only provide a true estimate of the midline when the midline is circular, but when the ring is bent an improved estimate has to be found. The method selected for calculating an updated midline position was to apply a low-pass filter to $\mathbf{m}_1(\theta)$ (necessary for the exclusion of quantisation and noise disturbances), and parametrise it as a function of its arc length, s, producing $\mathbf{m}_{s1}(s)$, calculate its normal direction, $\widehat{\mathbf{n}}(s) = \frac{d^2\mathbf{m}_{s1}/ds^2}{|d^2\mathbf{m}_{s1}/ds^2|}$ and then incrementally search along $\mathbf{m}_{s1}$ for the intersection of the normal with the inner and outer edges to find $\mathbf{r}_{si}(s)$ and $\mathbf{r}_{so}(s)$. The updated midline coordinate was then calculated as $\mathbf{m}(s) = (\mathbf{r}_{si}(s)+\mathbf{r}_{so}(s))/2$ and thickness taken as $T_s(s) = |(\mathbf{r}_{so}(s)-\mathbf{r}_{si}(s))|$.

A single point of material in the initially-uniform wall of the ring was selected to be the origin, corresponding to $s = 0$. A radial marker was applied to the ring's upper surface here. Other markers of a different colour were applied to the ring in an evenly-spaced radial spoke pattern on the initial ring, as shown in Figure 2. The markers were used to locate regularly-spaced fixed points of material in the circumference of the ring. The tangential centres of the markers were identified by looking for changes in hue and brightness along $\mathbf{m}$. The markers were drawn radially and used sparingly (12 here) so that they were visible even after large deformations of the wall.

Integrating the thickness along the arc length calculated the volume as a function of arc length (assuming constant axial height), $v(s) = \int_0^s T_s(\tau)d\tau$ and allowed the curvature, κ, (described in Section 2.2) to be calculated as a function of volume fraction, $v_f = v/V_{total}$, around the circumference instead of arc length. This provided $\kappa(v_f)$ for comparison with its targeted values in the final ring state, no matter the current ring diameter and thickness

[1] The midline is the closed curve running along the centre of the ring wall, equidistant between the inner and outer edges.

Fig. 2. A modelling clay ring with markers applied in a radial spoke pattern. The upper axial roll has been excluded for clarity. The inner and outer diameters of the ring were 45 mm and 85 mm respectively. In hot ring rolling the ring is usually glowing orange with heat, and orange modelling clay was used for its similar appearance.

which change the arc length for a segment of material, and is constantly changed during forming.

2.2 Estimating curvature

The curvature, κ, of the midline with respect to volume fraction around the unloaded [2] ring is the reference state to be controlled by the method presented here. When the midline curve is estimated parametrically as a function of arc length, s, such that $\mathbf{m}(s) = \mathbf{f}(x(s), y(s))$, the curvature, κ, is given by its usual form:

$$\kappa(s) = \frac{x'(s)y''(s) - y'(s)x''(s)}{((x'(s))^2 + (y'(s))^2)^{3/2}}. \tag{2}$$

The spatial resolution of the curvature measurement was limited by the quantisation error introduced by the nearest-pixel edge detection technique (chosen for computational efficiency), and the subsequent need for a low-pass filter.

To a greater or lesser extent, the rolls always apply loads that create some elastic deformation of the ring, which would be relaxed upon unloading. To accurately estimate the curvature around the whole midline in the unloaded ring, while the rolls are still applying loads, would require a computationally-complex model of the mechanics with accurate input parameters from additional sensors. This would be impractical, if not infeasible, to use in real-time applications. To estimate the ring curvature during forming, were the ring to be unloaded, an assumption was made that when the centre of the ring was coincident with the centre of the machine the curvature would be close to that of the unloaded ring. In this condition the elastic bending moment applied by the rolls should be a minimum, and therefore the measured curvature is close to the unloaded-ring curvature. Therefore the most accurate estimate of curvature is that taken when the centres of the ring and the RARR mill are coincident.

[2] The unloaded ring shape is the shape of the ring were it laid flat on a frictionless surface, not held by the roll pairs.

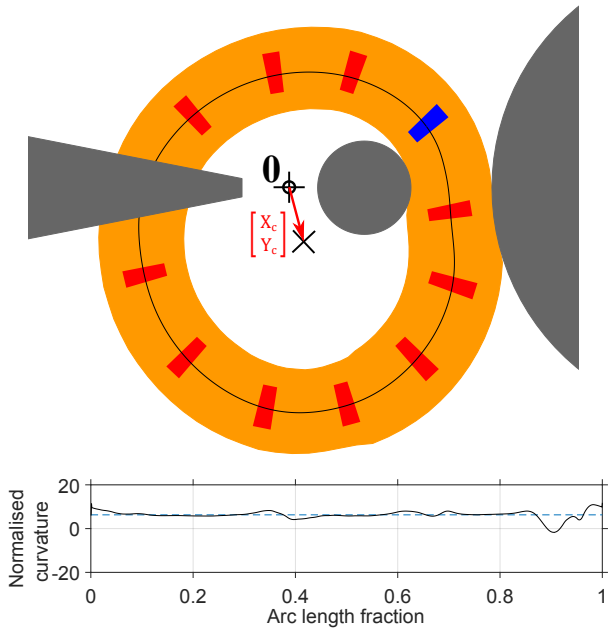

Fig. 3. A ring during an FE simulation where a plastic hinge has developed in the radial roll gap region.

3. PLASTIC CHANGE OF CURVATURE

3.1 Control of the plastic hinge rotation

As stated before, to alter the curvature of a segment of the ring wall, a plastic hinge is induced in the radial roll gap. The extent of the rotation of this hinge is controlled by the position of the ring centre, Y_c. As $|Y_c|$ increases, the rotation of the plastic hinge increases; an example of this is shown in Figure 3 where the $\times$ shows the current centre of the ring at $[X_c, Y_c]^T$. In this example the axial rolls had a higher feed speed than the forming roll. The plot shows the normalised curvature, $\kappa_n(s)$, for the ring - where the midline has been scaled to have a total length of 1. With this scaling a circular ring would have a constant curvature of 2π. Elsewhere in the ring the material does not undergo a large compressive state of stress and the bending moment is lower, which results in only elastic (recoverable) bending moments in segments not inside the radial roll gap.

3.2 Open-loop curvature control

The targeted ring centre position is defined as Y_t and this set point is used to control the rotation of the plastic hinge, and hence the curvature, of the ring wall currently in the radial roll gap. In conventional ring rolling, for circular curvature, the aim is pure centring and $Y_t = 0$. However, in shaped rings, to make Y_c follow a Y_t path the axial roll feed speed, v_a, relative to the forming roll feed speed, v_f, is changed using a proportional+integral control action using feedback from the error in Y_c, so $e_Y = Y_c - Y_t$ and $v_a = v_f + K_{vP}e_Y + K_{vI}\int e_Y$.

The plastic hinge was assumed to form over a short segment of arc length and to be unaffected by the bending of neighbouring segments as they passed through the gap. In reality, the hinge is not so tightly localised and the changes in curvature in neighbouring segments are not independent; hence the rate of change of a targeted

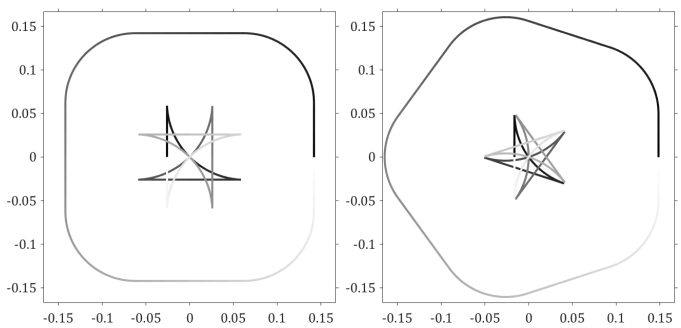

Fig. 4. Open-loop path trajectories of the machine centre scaled (normalised) with respect to length of the midline. The centre positions are plotted using shading to show the correspondence to the midline.

curvature profile is limited. The radius of the mandrel also applies a limit on the curvature - the inner edge of any bend cannot be sharper than the mandrel itself. In addition, the settling time for e_Y can be assumed to be very short, to allow neighbouring segments to be controlled independently, and in practice this assumption can be guaranteed by reducing the forming speed, but that may not be practical in all cases so an error in Y_c may remain. Given these constraints, relatively smooth ring shapes must be targeted. The test cases here were chosen so that these limits would not be violated and the Y_t path could then be calculated in a straightforward manner assuming independence of curvature along the midline.

Open-loop control of ring curvature was achieved by planning the path of Y_t as a function of the radial roll gap's position along $\mathbf{m}(s)$ before forming began. The mechanical principle used to construct the path was that the ring should move so that the radial roll gap direction (the X axis of the machine) would always be perpendicular to the midline, and that the midline would be held at a fixed distance from the machine centre.

Two examples of targeted midline shapes are shown in Figure 4, each with the path of the machine centre in the ring's frame of reference. The plots have been normalised so that they can be used throughout the forming of a ring by multiplying with the current midline length, and each example midline has a total length of one. These particular shapes were constructed as regular polygons with circular fillets. The sums of the lengths of the straight sides were chosen to be 0.5, resulting in curvature expected to be within the aforementioned limits. The necessary Y_t paths were then calculated from the midline perimeters using the geometry of the midline normals relative to the machine centre, as shown in Figure 5.

3.3 Closed-loop curvature control

More advanced control of the ring curvature could be achieved by using the measured curvature to calculate the centre-position offset required for each segment. The upcoming curvature value for a segment about to enter the radial roll gap region would be compared to its target value to find an error in curvature, κ_e. To achieve a greater change in curvature the open-loop value of Y_t would be multiplied by a factor. α_Y, calculated according to a PI control for that segment, $\alpha_Y = K_P\kappa_e + K_I \int \kappa_e$. This

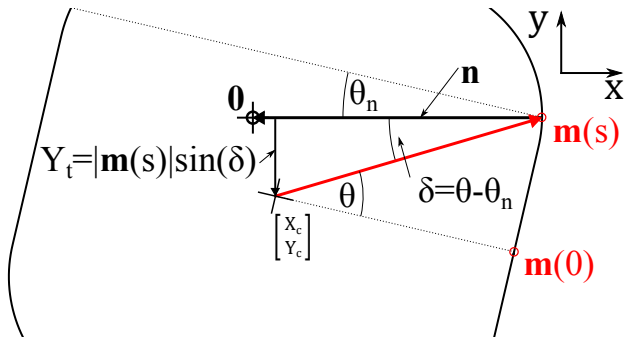

Fig. 5. Calculating the Y_t value at a particular value of s. When the radial roll gap is forming the segment of ring wall at $\mathbf{m}(s)$, $Y_t = |\mathbf{m}(s)|sin(\delta)$.

could be used to change curvature more quickly than using open-loop control and may be required if disturbances in the curvature were not removed using the open-loop path alone, such as when the ring has a variable wall stiffness. Trials using this feedback method are ongoing.

4. RESULTS

This section describes results from trials in finite element simulations and a desktop-scale RARR mill. The image processing software and the control algorithms were implemented in Matlab. In every trial the ring was initially 20 mm high, and had inner and outer diameters of 45 and 85 mm respectively. The ring in its initial marked state for the desktop-scale trials can be seen in Figure 2. The targeted wall thickness for the final shapes was 12 mm. The tangential velocity of the ring was set at 5 mm/s.

Finite element (FE) simulations of the RARR process were used to evaluate the curvature-control technique when applied to IN718, which is an industrially relevant alloy used in rolled-ring products for aerospace applications. In these simulations the results were periodically output and plotted to draw an image of the ring and the rollers. This image was then presented to the image processing software as if it were from a real camera. In this way, the control software for operating real hardware or simulated hardware could be shared by both systems. The frequency for outputting the simulation results was chosen to match that of the desktop-scale forming machine controller frequency, at 2 Hz. More details of the approach to modelling the industrial ring rolling process are given in Appendix A.

The upper plot of Figure 6 shows the results from a forming simulation targeting the square-shaped ring shown in Figure 4, and its final state is shown in the left hand image of Figure 7. The curvature was recorded when the ring centre coincided with the machine centre. It can be seen that the curvature evolution does tend to track the targeted curvature, but with a small offset in arc-length fraction, although it did not achieve the sharp changes in targeted curvature. The offset arc-length fraction was due to an error in the delay preview anticipated by the controller. However, this offset does not affect the resultant ring product (it still matches the targeted shape) because it had a uniform thickness throughout. This error could be corrected in future implementations. The error in matching the higher frequency content of the curvature target has been attributed to elastic springback, which

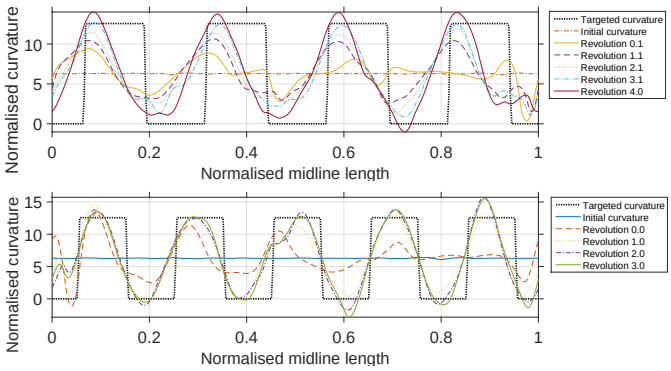

Fig. 6. The curvature evolution for an IN718 ring in a 3D FE simulation of the RARR process. The curvature has been normalised at each revolution so that a circular midline would have a curvature of 2π. The upper and lower plots show results for the square and pentagonal ring respectively.

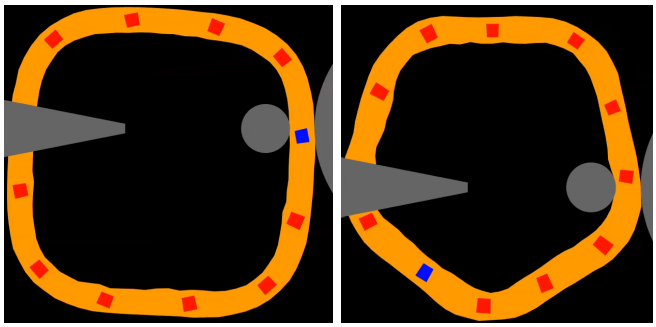

Fig. 7. The final states of the rings in the FE simulations with square and pentagonal curvature targets.

could be corrected with the implementation of the closed-loop controller.

The formation of the pentagon shape from Figure 4 was also simulated and the results are also shown in Figures 6 and 7. The differences between the targeted curvature and the actual curvature are attributed to the same factors as for the square ring. Together these two shapes demonstrate the potential range of products that might be made using this control procedure.

A desktop scale RARR mill, shown in Figure 8, (details of which can be found in Stanistreet et al. (2006)) was used to implement this control procedure while rolling a model material: modelling clay. Modelling clay behaves in a similar fashion to metals at elevated processing temperatures (of the order of half their melting temperature) Green (1951). Figures 9 and 10 show the results from the modelling-clay trials for the square and pentagonal shapes of Figure 4. A delay, due to the total time required to acquire the image, apply the image processing algorithms, extract the geometrical data and compute the actuation required for the next step was unavoidable. With a desktop PC running at 3.4 GHz with 16 GB of RAM, using an HD USB camera this delay was of the order of 400 ms. The controller therefore looked ahead at the zone approximately 2 mm ahead of the centre of the radial roll gap when computing the required actuation, but in practice this was insufficient to compensate for the finite settling

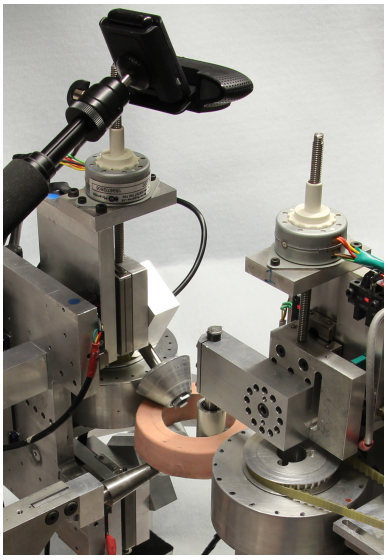

Fig. 8. The desktop-scale RARR mill used to perform ring rolling experiments on modelling clay. The mandrel was supported from below in the trials here.

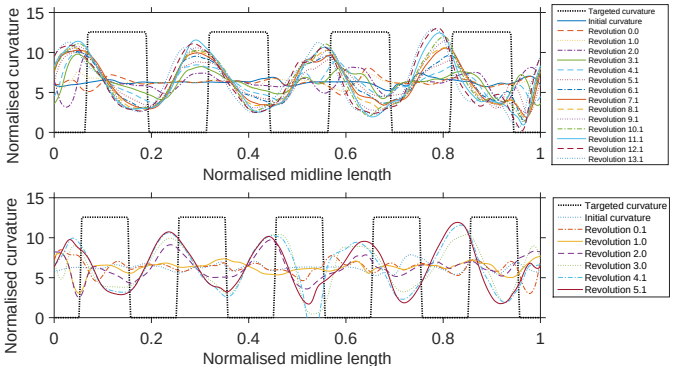

Fig. 9. The curvature evolution for RARR of modelling clay. The upper and lower plots show results for the square and pentagonal target shapes respectively. The curvature has been normalised at each revolution so that a circular midline would have a curvature of 2π.

time of e_Y and should be set larger in future. Again, it can be seen that the curvature evolution does track the targeted evolution, but with an offset in arc length, this time even greater than in the FE simulation results, of the order of 7% of the midline length. The preview of the controller could be adjusted to compensate for this, but the final rings still have the desired target shape.

5. CONCLUSION

Ring rolling is an efficient method for producing high quality ring products. Controlling curvature of the rings during the process has, conventionally, been limited to achieving circular shapes. In this work we have demonstrated in finite element simulations of industrial rolling conditions, and in modelling clay experiments, that curvature control can be achieved in a RARR configuration without using guide rolls. This capability can be used to create non-circular ring shapes using existing RARR rolling hardware with additional sensing and control.

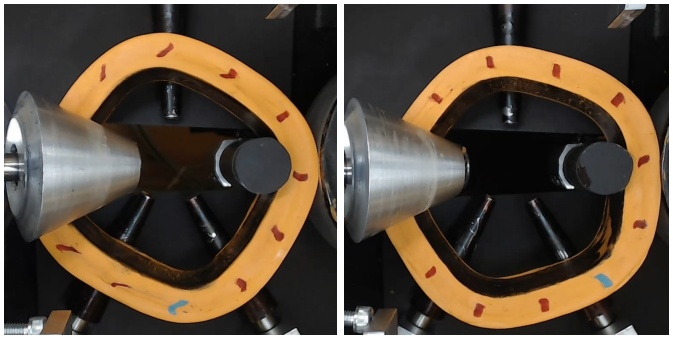

Fig. 10. The final states of the clay rings with square and pentagonal curvature targets.

Both a square ring and a pentagonal ring were created as examples in this work, but a continuous variety of shapes within the limits of the process can be formed using the control technique described here. When combined with new forming processes such as variable-wall-thickness control, these methods greatly extend the range of shapes achievable in radial-axial ring rolling.

REFERENCES

(1988). *ASM Metals Handbook Volume 14: Forming and Forging*. ASM International.

Allwood, J.M., Tekkaya, A.E., and Stanistreet, T.F. (2004). The Development of Ring Rolling Technology Part 2 : Investigation of Process Behaviour and Production Equipment. 489–505.

Allwood, J.M., Tekkaya, A.E., and Stanistreet, T.F. (2005). The development of ring rolling technology. *Steel research international*, 76(2-3), 111–120.

Arthington, M.R., Cleaver, C., Allwood, J., and Duncan, S. (2014). Real-time measurement of ring-rolling geometry using low-cost hardware. In *2014 UKACC International Conference on Control, CONTROL 2014 - Proceedings*, July, 603–608. IEEE.

Arthington, M., Cleaver, C., Allwood, J., and Duncan, S. (2015). Measurement and control of variable geometry during ring rolling. In *IEEE Multi-Conference on Systems and Control*, 1448–1454. Sydney, Australia.

Cheng, L., Xue, X., Tang, B., Liu, D., Li, J., Kou, H., and Li, J. (2014). Deformation behavior of hot-rolled IN718 superalloy under plane strain compression at elevated temperature. *Materials Science and Engineering: A*, 606, 24–30.

Green, A.P. (1951). The Use of Plasticine Models to Simulate the Plastic Flow of Metals. *The philosophical magazine*, 42(327), 365–373.

Hibbit, Karlsson, and Sorensen (2007). *ABAQUS/Standard Analysis User's Manual*.

Meier, H., Briselat, J., Hammelmann, R., and Flick, H. (2010). Image Processing Methods for Online Measurement in Radial-Axial Ring Rolling. *Proceedings of the 36th International MATADOR Conference*.

Moon, H.K., Lee, M.C., and Joun, M.S. (2008). Predicting polygonal-shaped defects during hot ring rolling using a rigid-viscoplastic finite element method. *International Journal of Mechanical Sciences*, 50(2), 306–314.

Stanistreet, T.F., Allwood, J.M., and Willoughby, a.M. (2006). The design of a flexible model ring rolling machine. *Journal of Materials Processing Technology*, 177(1-3), 630–633.

Yeom, J.T., Lee, C.S., Kim, J.H., and Park, N.K. (2007). Finite-element analysis of microstructure evolution in the cogging of an Alloy 718 ingot. *Materials Science and Engineering: A*, 449, 722–726.

Zhou, L.X. and Baker, T.N. (1994). Effects of strain rate and temperature on deformation behaviour of IN 718 during high temperature deformation. *Materials Science and Engineering: A*, 177(1-2), 1–9.

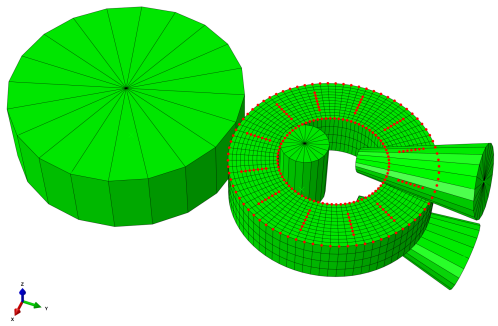

Fig. A.1. The 3D finite element mesh used to simulate industrial ring rolling conditions.

Appendix A. FINITE ELEMENT MODELLING PROCEDURE

Implementation of the curvature-control technique using industrial production conditions was tested in a virtual ring rolling system developed using a general purpose finite element software, Abaqus (V6.14-1), Hibbit et al. (2007). In this framework, a 3D coupled thermo-mechanical FE model was developed to simulate the RARR process with full control of all degrees of freedom of all rolls. Figure A.1 shows the 3D FE model for the RARR process, in which all rolls are treated as rigid surface bodies, and the control of their movement is implemented in a user defined subroutine (UAMP). The ring was meshed by coupled thermo-mechanical hexahedral elements (C3D8RT). An adaptive mesh procedure throughout the whole domain was used to maintain a high quality mesh when large deformation occurred during the RARR process. The coordinates of the highlighted nodes in Figure A.1 defined on the top surface of the ring are output for plotting to create the image for the image processing software in Matlab. The model is solved using a dynamic-explicit solver with a mass scaling factor of 200 to speed up the computation time. The material used in the simulation was IN718, which is the most frequently used nickel-based superalloy in production of seamless rings for the aerospace and energy industries. Mechanical behaviour properties for this material can be found in Zhou and Baker (1994), Yeom et al. (2007) and Cheng et al. (2014). The ring temperature of these simulations was 1100 °C and a Sellars-Tegart relationship was employed to ensure that the material behaviour could be modelled accurately in the range 950 - 1120 °C.